Nanoscale

High Broadband Photoconductivity of few-layered MoS_2 Field-effect Transistor Measured in Multi-terminal Method: Effect of Contact Resistance

Journal:	*Nanoscale*
Manuscript ID	NR-COM-10-2020-007311
Article Type:	Communication
Date Submitted by the Author:	13-Oct-2020

Complete List of Authors:	Das, Priyanka; Jackson State University, Chemistry, Physics and Atmospheric Science Nash, Jawnaye; Jackson State University, Department of Chemistry, Physics and Atmospheric Science Webb, Micah; Jackson State University, Chemistry, Physics and Atmospheric Science Burns, Raelyn ; Jackson State University, Chemistry, Physics and Atmospheric Science Mapara, Varun; University of South Florida, Physics Ghimire, Govinda; Jackson State University, Chemistry, Physics and Atmospheric Science Rosenmann, Daniel; Argonne National Laboratory, Divan, Ralu; Argonne National Laboratory, Center for Nanoscale Materials Karaiskaj, Denis; University of South Florida, Physics McGill, Stephen; National High Magnetic Field Laboratory, Sumant, Anirudha; Argonne National Laboratory, Centre for NanoMaterials Dai, Qilin; Jackson State University, Department of Physics Ray, Paresh; Jackson State University, Chemistry and Biochemistry Tawade, Bhausaheb; Howard University, Chemistry Raghavan, Dharmaraj; Howard University, Karim, Alamgir; University of Houston Pradhan, Nihar; Jackson State University, Physics; National High Magnetic Field Laboratory, Condensed Mater Physics

High Broadband Photoconductivity of few-layered MoS_2 Field-effect Transistor Measured in Multi-terminal Method: Effect of Contact Resistance

Priyanka Das[1], Jawnaye Nash[1], Micah Webb[1], Raelyn Burns[1], Varun N. Mapara[2], Govinda Ghimire[1], Daniel Rosenmann[3], Ralu Divan[3], Denis Karaiskaj[2], Stephen A. McGill[4], Anirudha V. Sumant[3], Qilin Dai[1], Paresh C. Ray[1], Bhausaheb Tawade[5], Dharmaraj Raghavan[5], Alamgir Karim[6], and Nihar R. Pradhan[1,4]

[1]*Layered Materials and Device Physics Laboratory, Department of Chemistry, Physics and Atmospheric Science, Jackson State University, Jackson, MS 39217, USA*

[2]*Department of Physics, University of South Florida, Tampa 33620, USA*

[3]*Center for Nanoscale Materials, Argonne National Laboratory, 9700 S-Cass Avenue, Lemont, IL-60439, US*

[4]*National High Magnetic Field Laboratory, Tallahassee, FL 32310, USA*

[5]*Department of Chemistry, 525 College Street, NW, Howard University, Washington DC 20059, USA*

[6]*Department of Chemical & Biomolecular Engineering, University of Houston, S333 Engineering Bldg 1, 4726 Calhoun Rd, Houston, TX 77204, USA*

Among the layered two dimensional semiconductors, molybdenum disulfide (MoS_2) is considered to be an excellent candidate for applications in optoelectronics and integrated circuits due to the layer-dependent tunable bandgap in the visible region, high ON/OFF current ratio in field-effect transistors (FET) and strong light-matter interaction properties. In this study, using multi-terminal measurements, we report high broadband photocurrent response (R) and external quantum efficiency (EQE) of few-atomic layered MoS_2 phototransistors using multi-terminal measurements, fabricated on a SiO_2 dielectric substrate and encapsulated with a thin transparent polymer film of Cytop. The photocurrent response was measured using a white light source as well as monochromatic light of wavelength λ = 400 nm - 900 nm. We measured responsivity in 2-terminal configuration as high as $R = 1\times10^3$ A/W under white light illumination with optical power P_{opt} = 0.02 nW. The R value increased to 3.5×10^3 A/W when measured using a 4-terminal configuration. Using monochromatic light on the same device, the measured values of R were 10^3 and 6×10^3 A/W under illumination of λ = 400 nm when measured in 2- and 4-terminal methods, respectively. The highest EQE values obtained using λ = 400 nm were 10^5 % and 10^6 % measured in 2- and 4-terminal configurations, respectively. The wavelength dependent responsivity decreased from 400 nm to the near-IR region at 900 nm. The observed photoresponse, photocurrent-dark current ratio (PDCR), detectivity as a function of applied gate voltage, optical power, contact resistances and wavelength were

measured and are discussed in detail. The observed responsivity is also thoroughly studied as a function of contact resistance of the device.

Keywords: Phototransistors, Molybdenum disulfide, responsivity, quantum efficiency, detectivity.

Electronic address: Corresponding email: nihar.r.pradhan@jsums.edu

I. INTRODUCTION

High sensitivity photodetectors showing fast responses to optical fields capable of converting optical inputs to electrical signals, are the building blocks of many multifunctional optoelectronic devices. These components find broad applications in consumer electronics, optical communications [1], sensors in supermarkets, self-driving cars, bioimaging and living cell inspection [2-5], infrared imaging, weather monitoring [6] and cameras [7]. Despite the tremendous growth in research during the past few years, Si-based photodetectors are difficult to replace and still comprise the largest share of the electronic industry due to their low-cost and ease-of-integration in devices. Photodetectors beyond CMOS-based technology with reference to the scaling limit, speed and device density show limitation for applications in near-infrared or far-infrared regions. Currently many infrared CMOS photodetectors are based on InGaAs or HgCdTe, which suffer from high cost of manufacturing. Furthermore, CMOS-based photosensors may not be a good candidate for future technologies, like wearable electronics, due to their geometric limitations and difficulty in integration to thin, flexible devices.

Two-dimensional, layered materials consisting of single-to-few atomic layers show potential for applications in flexible electronics due to their transparency and flexibility. In addition, they offer a unique opportunity to expand optical sensitivity beyond the limit of CMOS devices. Among the various 2D materials investigated for their photodetection properties, transition metal dichalcogenides (TMDs) are at the forefront due to their tunable bandgaps in the UV-visible regions [8-10]. They show strong light-matter interactions due to the presence of Van Hove singularities in the density of states. This is due to the localized nature of the electronic wave-functions of the d-orbital in transition metals and p-orbitals of chalcogen atoms [11-13].

MoS_2 is one of the most studied materials among the TMDs family due to its common availability and stability in ambient conditions. Many photoconductivity studies of MoS_2 are focused only on the visible region of the solar spectrum, reportedly showing a wide range of photoresponsivities spanning from low values as 0.5 mA/W to values as high as 880 A/W and being highly dependent upon the applied gate voltage, source-drain voltage and incident optical power [14-16]. The photoresponsivity, (R), is inversely dependent on the applied optical power ($R \propto P_{opt}^{-\gamma}$) [15, 17-19]. It is also linearly dependent on the applied drain-source voltage (V_{ds}). The response time is one of the crucial figure-of-merit for photodetectors used in fast/slow and weak signal detection. Many 2D semiconducting systems show response times as large as *ms* to as small as μs [14-16, 18, 19]. The response time depends upon the area of the detector, laser power and the method of measurement. Two-dimensional semiconductors not only show high responsivity at room temperature but also yield a stable photodetection characteristic under extreme conditions such as wide temperature range (20^o C to 400^o C) and high

radiation environment [20-22]. These properties make 2D semiconductor-based photosensors especially promising for optoelectronics.

Many photodetectors operate either in the visible region of the solar spectrum or using monochromatic laser sources and show extremely high responsivity, external quantum efficiencies (EQE) and excellent low-signal detection [11, 17, 18, 23-27]. However, multifunctional applications could be explored using single device components if the photosensor worked in broad spectral range instead of just a single wavelength. But to our knowledge only a limited number of studies on broadband photodetection in 2D material-based devices have been reported. Choi and coworkers [28] reported broadband photodetection using a 60 nm thick MoS_2 photodetector fabricated on a Al_2O_3 dielectric substrate. They observed broadband photoresponsivity of ~ 50 mA/W in the range of 450 nm to 750 nm. The responsivity reported by Choi et al. is smaller than the reported broadband responsivity of 0.5 A/W announced by Tsai et al. in the range of 400 nm to 700 nm [29]. Recently, Lee and coworkers [30] reported gate voltage dependent broadband photoresponsivity on a graphene-contacted few-layered MoS_2 phototransistor. They observed R~ 10^{-3} A/W - 1 A/W from 450 nm to 800 nm when the transistor operated in the OFF state. This value increased substantially by three orders-of-magnitude to 10^3 A/W when the transistor operated in the ON state at applied gate voltage, V_g = 20 V. The graphene contact on MoS_2 could be responsible for the high carrier conduction/injection from the MoS_2 channel to the graphene-contact electrodes. There are very few studies elucidating the possible broadband optical response of MoS_2 phototransistors. Some of these responsivities are still poor in the whole spectral region or particularly in the IR region. The intrinsic photoresponse is still enigmatic due to the various factors involved in the device fabrication such as contact resistance between the metal contact and semiconductor channel which forms Schottky barriers and limits efficient charge-carrier injection from the semiconductor to the metal. The quality of the material is also an important factor as impurity scattering could further reduce the photocurrent response. The environmental conditions during the measurements could also cause the poor responsivity, for example if the device is exposed to the ambient and water vapor on the surface of 2D channel inhibiting the photocurrent generation.

In this work, we explored the intrinsic broadband photoconductivity of a ~ 10-15 atomic layered MoS_2 photo-transistors from visible-to-IR region fabricated on a 285 nm thick SiO_2 coated on Si substrate. We measured the intrinsic optical conductivity using multi-terminal (4-terminal) measurements, which showed a much higher response compared to the conventional 2-terminal measurements. The photoconductivity was evaluated using both white and monochromatic light, yielding a high photoresponsivity as a function of gate voltage, incident optical power and wavelength.

II. SYNTHESIS AND DEVICE FABRICATION

We synthesized bulk MoS_2 crystals through a traditional chemical vapor transport (CVT) technique [31-33] using Iodine as the transport agent. We exfoliated single- to several atomic-layers thick MoS_2 flakes from a bulk single crystal using the mechanical scotch tape exfoliation technique (Supporting information Fig. S1) and characterized via Raman microscopy to verify the quality of the crystal. Raman spectroscopy of single-layer to seven-layers thick flakes are presented in Fig. S1(b) along with the Raman spectrum of bulk MoS_2. We fabricated the FET devices using few-atomic-layer MoS_2 (12 nm thick device presented below and a second 15 nm thick device presented in the Supplemental Information section) on a clean Si substrate thermally deposited with a 285 nm thick SiO_2 layer. We fabricated several multilayered MoS_2 FETs using a Microtech Laser writer (Model # LW405) and metal contacts (5 nm Cr/ 80 nm Au) were deposited using a Lesker e-beam evaporator with a base pressure in the low 10^{-8} Torr range. After the devices were fabricated the channel area was covered with a thin layer of Cytop (transparent thin polymer film) to prevent the MoS_2 layers from direct exposure to the ambient air/oxygen environment. Our previous experience suggested the long durability of the device when encapsulated or coated with Cytop [34-36].

III. RESULTS AND DISCUSSION

Figure 1 (a) shows the schematic of the device with measurement scheme. Figure 1 (b) shows the optical image of the device with 6 contacts fabricated on the Si/SiO_2 substrate. The thickness of the MoS_2 layer is 12 nm as measured by atomic force microscopy. Highly p-doped Si substrate was used for the back gate to control the charge carrier density inside the channel. Figure 1 (c) shows the drain-source current (I_{ds}) as a function of drain-source voltage (V_{ds}) measured using 2-terminals, source (S) and drain (D) contacts. The I-V curve shows linear dependencies between 0 to 200 mV and at all applied gate voltages without showing any sign of nonlinearity even though there is a possibility of schottky barrier formation between the semiconductor and metal junction. This linear I-V behavior is due to the thermionic emission process at room temperature due to thermal energy where the carriers can be easily promoted into the conduction bands from the valence band. Figure 1 (d) shows the I_{ds} vs V_{ds} measured using 4-terminal configurations from the same device that yields a much higher drain current (4 times higher) compared to the current measured from 2-terminal configurations. This enhanced output current measured by the 4-terminal method is due to the elimination of the contact resistance associated with the 2-terminal measurement. 2D semiconducting materials composed of single to few-atomic layers are prone to form Schottky contacts due to the pinning of Fermi level (FLP) at the interface, which arises from the difference in the work function between the metal and semiconductor [37].

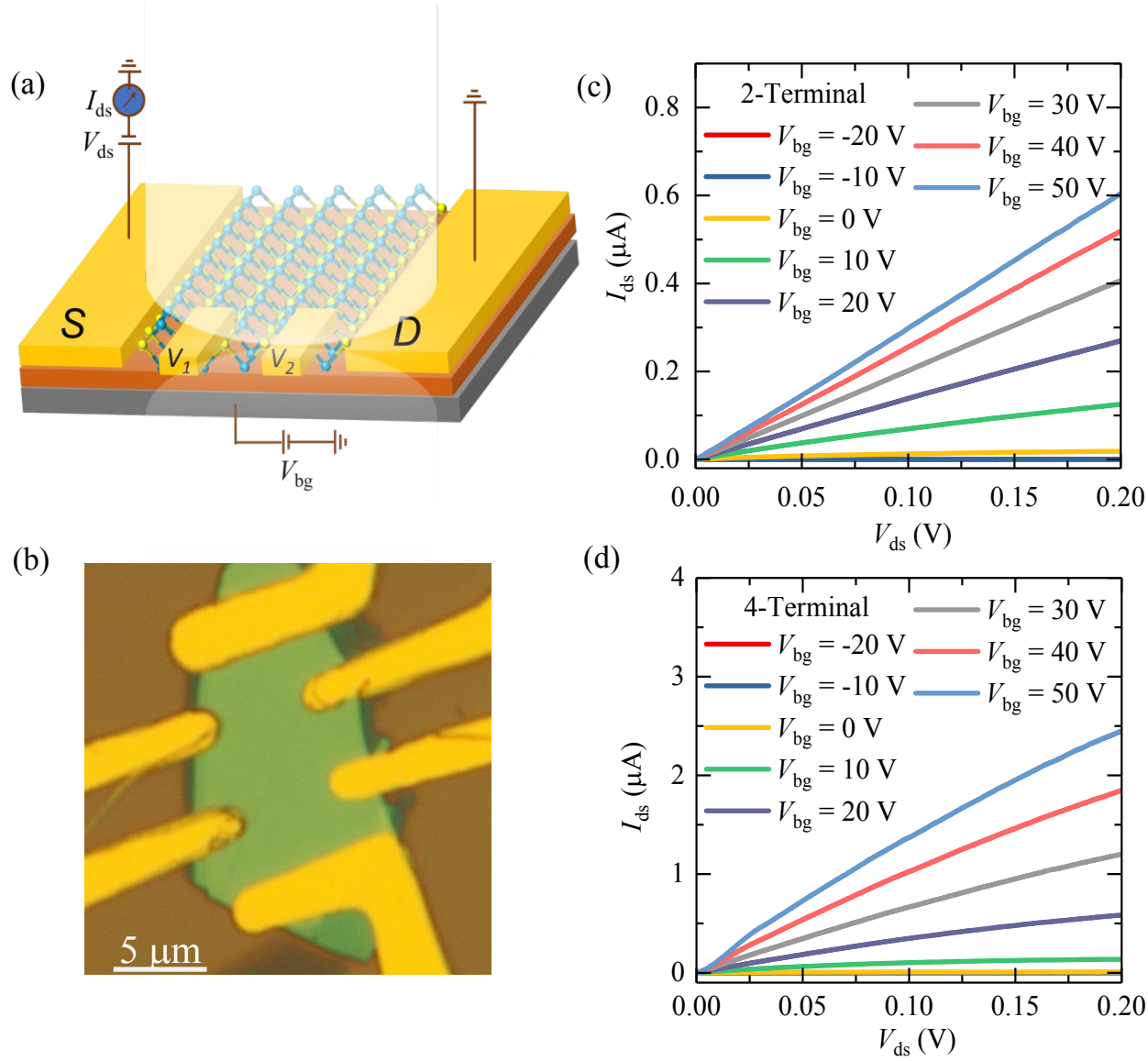

FIG. 1: (a) Shows the graphic design of the device with measurement scheme. 2-terminal measurement was performed using S and D contacts and 4-terminal measurement were performed using S and D as current injection and V_1 and V_2 are voltage sense contacts. (b) Depicts the optical image of one of the ~12 nm thick MoS_2 device with multiterminal contacts using Cr/Au (5 nm /80 nm) metal contacts fabricated on the 285 nm SiO_2 layers deposited on p-doped Si substrate. (c) and (d) displays the I_{ds} as a function of V_{ds} at several constant gate voltages using 2- and 4-terminal configurations, respectively.

The work function of few-layered MoS_2 is ~ 5.2 eV and for Cr is 4.5 eV [38]. Theoretically it could form a Schottky barrier height of ~ 0.7 eV. This barrier height may vary with the number of semiconducting layers [37]. For monolayer MoS_2 contacts with 3D metals, strong pinning is found at the metal-semiconductor (M-S) interface [37]. The FLP originates from several factors such as the formation of an electric dipole at the interface due to change of the charge distribution at the junction and metal & defects/disorder induced gap states [39, 40]. The pinning may be less pronounced in a multilayered MoS_2 compared to the single layer. The charge accumulation in multilayer is larger than on a single layer, which could reduce the pinning effect.

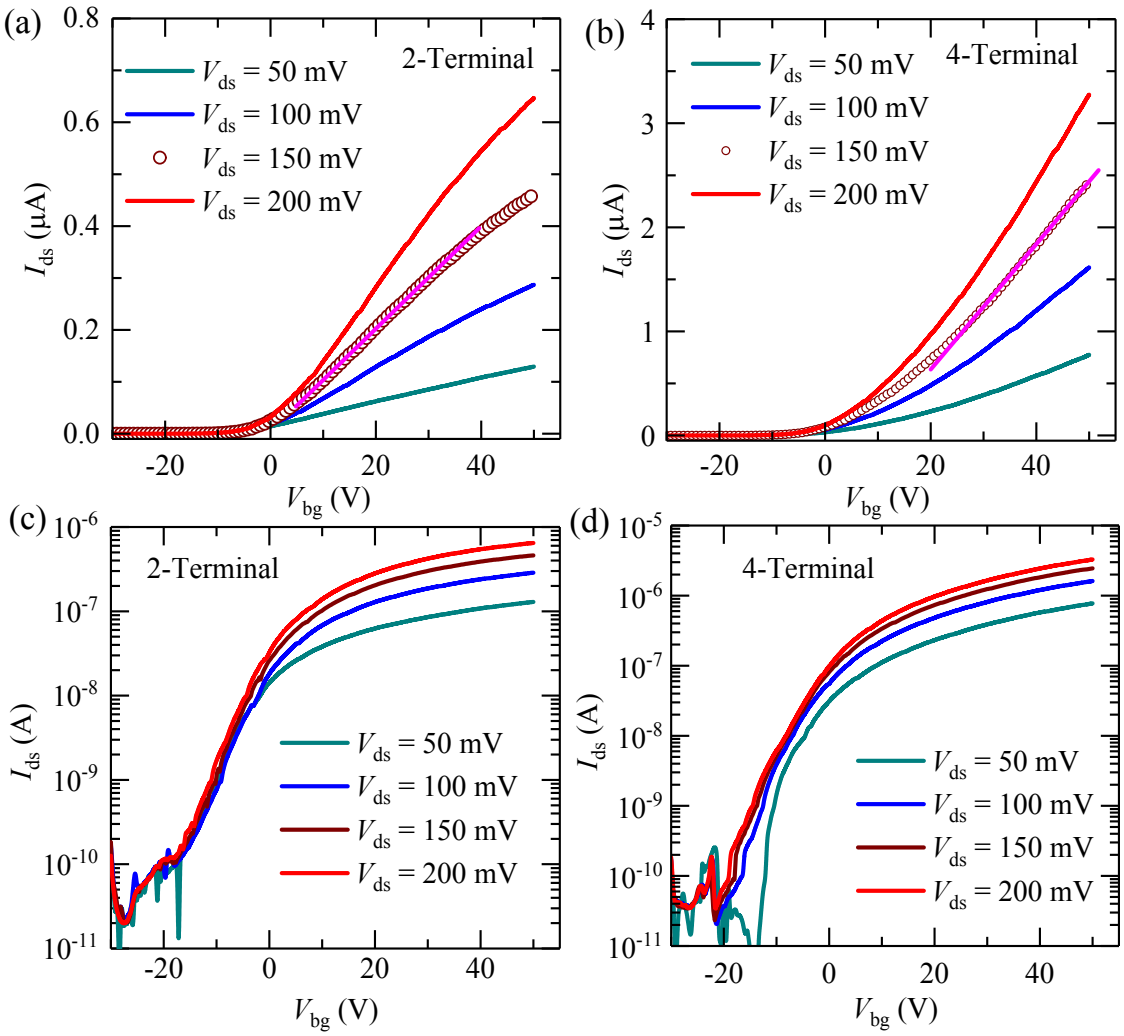

FIG. 2: (a) and (b) display the I_{ds} as a function of V_{bg} at several constant V_{ds} measured in 2- and 4-terminal, respectively. The magenta solid line is the linear-fit for one of the curves at V_{ds} = 150 mV. (c) and (d) are the same pair of graphs shown in (a) and (b) but in logarithmic scale.

Figure 2 displays the transport characterization of MoS_2 FET. I_{ds} as a function of V_{bg} at fixed V_{ds} = 50 mV, 100 mV, 150 mV and 200 mV were measured using 2-terminal method is shown in the Fig. 2 (a). The FET shows minimum current at applied negative V_{bg} which indicates the OFF state of the transistor and when the gate voltage is swept to the positive direction, current increases exponentially, which confirms the ON state of the transistor. The FET behavior as a function of gate voltage shows minimum current at negative applied gate voltage and increases exponentially when swept towards the positive gate voltage indicating that the MoS_2 crystal shows high electron doping as previously reported by several research groups [41-44]. The high electron doped behavior in MoS_2 is found to originate from the high density of S vacancy in MoS_2 crystals [45, 46]. The magenta color lines shown in the I_{ds} vs V_{bg} for both 2- and 4-terminal measurements of Fig. 2 (a) and (b) are the linear-fit to one of the curves

at V_{ds} = 150 mV used to extract the slope of the curve. The charge carrier mobility was calculated using the standard MOSFET transconductance formula as shown below and using the slope values of $\frac{d(I_{ds})}{d(V_{bg})}$.

$$\mu^{2T} = \frac{L}{W} \times \frac{1}{C_i} \times \frac{d(I_{ds})}{d(V_{bg})} \times \frac{1}{V_{ds}} \quad (1)$$

where L = 13.7 μm is the channel length of the device between source and drain contacts (used for 2-terminal method), W = 6 μm is the width and C_i is the capacitance per unit area of the device. For 285 nm thick SiO_2 layer, calculated $C_i = 12.738 \times 10^{-9}$ F. The calculated 2-terminal mobility for our few layered MoS_2 devices is 14 cm^2/Vs. Figure 2 (b) displays the same data as 2 (a) but measured in 4-terminal method. We used $\mu^{4T} = \frac{l}{W} \times \frac{1}{C_i} \times \frac{d(I_{ds} - I_o)}{dV_{bg}} \times \frac{1}{V_{ds}}$, where l = 4.8 μm is the channel length between two voltage leads V_1 and V_2 to calculate the carrier mobility from the 4-terminal measurements as the channel length for this measurement is the length between two voltage probes V_1 and V_2 and not between the "S" and "D" contacts. The voltage drop measured or sense between V_1 and V_2 contacts in 4-terminal method and the mobility extracted using the same drain-source voltage V_{ds} = 150 mV, (same as V_{ds} for 2-terminal measurements). Similar to I_{ds} vs V_{ds}, the current measured using the 4-terminal method in gate sweep is also much higher (~ 5 times higher) than that obtained through the 2-terminal method. The 4-terminal mobility μ^{4T} = 33 cm^2/Vs is larger than that given by the 2-terminal mobility [41]. Similar mobility was extracted from a second device #2 in 2- and 4-terminal configurations (see supporting information section Fig. S5). The I_{ds} as a function of V_{bg} plot shown in Fig. 2 (a) and 2 (b) are again depicted in Fig. 2 (c) and (d) but in logarithmic scale to visualize the ON/OFF current ratio of the device. The current ratio of the FET between ON and OFF states is 10^5, which is similar to many reported multilayer MoS_2 FET [41, 47-49]. The ON and OFF current ratio is expected to increase as the applied V_{ds} increases, but we limited the V_{ds} to 200 mV for the safe operation of the device and to avoid damaging it before the optical measurements performed at a later stage. The I_{ds} value saturated above the gate voltage V_{bg} = 5 V and suggested that accumulated free charge carriers near the source contact were swept across the depletion region by the applied electric field and current remained nearly constant. The saturation of current was because of the fully depleted channel and limited to the contact resistance for the measurements in 2-terminal configurations. The 4-terminal measurements have the same effect of depletion of the channel, but higher current saturation was observed due to the elimination of contact resistance.

The electrical and optical transport properties measured from a second device #2, given in supporting information, showed photoconductivity properties similar to device #1. The FET transport measurement of device #2 was performed with the gate sweep from -20 V to 15 V. Device #2 showed threshold gate voltage V_T ~ -10 V, which was different from the threshold gate voltage of device #1,

$V_T \sim 0V$, which can be obtained by linear extrapolation from the I_{ds} vs V_{bg} graph, Fig. 2 (a) or 2 (b). Both devices showed similar ON/OFF current ratios and threshold voltage swings. The threshold gate voltage difference could be due to the thickness difference between the two devices, where device #1 is 12 nm thick and device #2 is 15 nm thick. Additionally, some photoresist polymer may be leftover at the interface between semiconductor and metal junction during fabrication process, which could also result in differences in FET characterization from one device from the other.

In order to study the optical properties of the device the white light source (Motic MLC-150 C halogen fiber optic illuminator) was fed through a microscope lens. The optical power was initially measured with a power meter at the sample position while varying the intensity of the light under dark room condition. Figure 3 displays the overall optical response of our multilayer MoS_2 phototransistor using white light illumination. Figure 3 (a) and (b) show the drain-source current as a function of applied gate voltage at different illuminating optical power including the dark current (I_{dark}). I_{dark} was measured when the illuminator is turned OFF and in dark room environment. In the following optical measurements, we commonly used bias voltage and optical power. The bias voltage is applied between the source and drain to drive the carrier from source contact to drain contact. The optical power is the power provided by the illuminated light on the top of the channel which generates electron-hole pairs within the semiconducting channel, and the electrons and the holes will move towards the drain or source by applied bias voltage.

The observed drain-source current increases with increasing optical power from 0.02 nW to 2.27 nW in both 2-and 4-terminal measurements. We calculated the photogenerated current, I_{ph} by subtracting the dark current from the values of I_{ds} when measured with illuminated light called I_{light}, ($I_{ph} = I_{light} - I_{dark}$). I_{light} is equal to I_{ds} but under illumination. We saw a significant enhancement of photocurrent when measured using the 4-terminal configuration compared to 2-terminal configuration (Supporting Fig. S2). The threshold voltage decreases and the current increases as a function of increasing optical power, indicating photogating effect in our device similar to the results previously reported for InSe and ReS_2 phototransistor devices [19, 50]. Photogating phenomena may arise from charge traps at the interface between MoS_2 layers and SiO_2. Electron-hole pairs created by photoexcitation are pulled towards the electrode by the applied voltage. In MoS_2, photoconduction is facilitated by majority of charge carrier electrons and minority carrier holes. Holes can be easily trapped at the interface producing photo gain while an electron can move through the external circuit many times before it recombines with a hole. This enhances the photogain of the device [19]. This photogating effect may also increase the electron-hole recombination time since more positive charge carriers are generated

with increasing optical power, filling the trap states. We extracted the responsivity of the device using the relation $R = \frac{I_{ph}}{P_{opt}}$. P_{opt} is the optical power illuminated on the channel area.

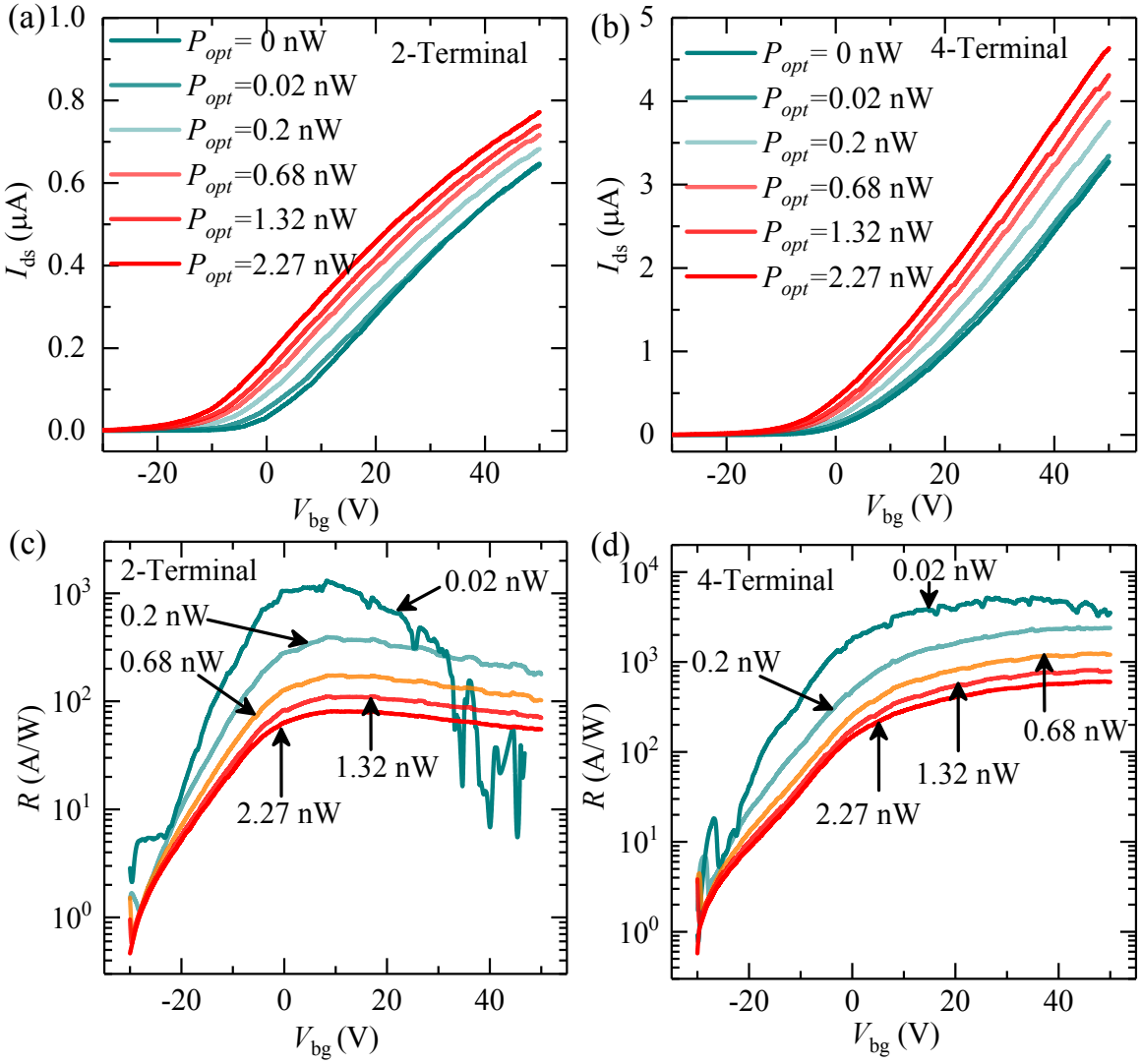

FIG. 3: (a) and (b) display the drain-source current as a function of applied back gate voltage at illuminated optical power P_{opt} = 0.02 nW, 0.2 nW, 0.68 nW, 1.32 nW, 2.27 nW measured in 2- and 4-terminals respectively. (c) and (d) shows the 2-and 4-terminal photoresponsivity of the device as a function of gate voltage at constant input optical power.

However taking the device geometry into account, we calculated the optical power incident on the sample area using the formula $P_{opt} = \frac{P}{\pi r^2} \times A$, where P is the total power measured using a power meter, r is the radius of the spot and A is the area of the sample. In 2-terminal measurements for all the applied power, R increases with increasing gate voltage and reaches to a maximum value between 0 V to 10 V of applied gate voltage. This indicates that the number of electron-hole pairs generated increases with increasing gate voltage or increasing accumulation of carriers at the interface. The number of generated carriers saturates above a certain gate voltage [>5 V, as seen from Fig. 3 (c) and

Fig. 3 (d)] and limited by contact resistance. This results in the saturation of electron-hole pair generation and the decrease in responsivity with further increasing the power. The responsivity measured in 4-terminal configuration is depicted in Fig. 3 (d) is much larger than that measured in 2-terminal configuration due to the elimination of the contact resistance. The highest responsivity obtained is 6×10^3 A/W at $P_{opt} = 0.02$ nW. This value is similar to the high responsivity reported in monolayer MoS_2 but at higher applied $V_{ds} = 8$ V [15]. The phototransport parameters such as responsivity, EQE, PDCR and detectivity values obtained from this study are compared to the reported results from several research groups and presented in supporting information section Table -1. The responsivity saturated at high gate voltage in 4-terminal measurements, whereas the responsivity decreased slowly above $V_{bg} = 5$ V in 2-terminal configuration [Fig. 3 (c)]. The decreasing trend of responsivity for the 2-terminal method could be caused by heating of the contacts due to the contact resistance. The saturation of photoresponsivity in 4-terminal measurements [Fig. 3 (d)] suggested the photocarrier generation in the channel became saturated. Thus, the further increase of gate voltage did not increase the responsivity of the device. In the 2-terminal configuration not only the channel was depleted but also the photogenerated carriers were limited due to the effects of contact resistance, which limited the current flow and decreased the current with increasing gate voltage. A similar value for the responsivity was measured on the second MoS_2 device #2 which is presented in the supporting information section (Fig. S7).

In the supporting information section, Fig. S3 shows R at $V_{bg} = 0$ V and 10 V as a function of illuminated optical power under white light in logarithmic scale. The highest responsivity obtained from our few-layered MoS_2 transistors when measured using a two-terminal configuration is 10^3 A/W for $V_{bg} = 0$ V when the transistor is in its ON state and under an illumination power $P_{opt} = 0.02$ nW [Fig. S3 (a)]. We fitted the responsivity using power law ($R \propto P^{-\gamma}$) as a function of P_{opt}. From this fitting, we obtained the exponent $\gamma = 0.5$ - 0.6. The same power law exponent also obtained from the 4-terminal data display in Fig. S3 (b). The decrease of responsivity as a function of optical power in sublinear manner is due to the charge trap which can occur at the interface between MoS_2 and SiO_2 substrate. SiO_2 has many dangling bonds [51] and can be the primary source of charge traps at these defect sites. The influence of charge trap could be significant in these 2D materials where surface to volume ratio is large, which leads to the large responsivity. The presence of defects (missing S atoms) [46] could be another reason for this high responsivity due to the charge trap on the defect sites.

The contact resistance has considerable effect on the transport properties of the device, particularly in 2D material based devices as we saw in previous sections. The lower the contact resistance, the better is the device performance which increases the current injection rate from semiconducting channel to the metal contacts and vice versa [41, 52]. Figure 4 shows the contact resistance extracted from the 2- and 4-terminal photocurrent measurements using the following formula

$$R_c = \frac{\frac{V_{ds}}{I_{2T}} - \frac{V_{ds}}{I_{4T}}}{2} = \frac{R_{2T} \quad R_{4T}}{2} \qquad (2)$$

Where V_{ds} is the drain-source voltage applied and measured between source and drain contacts for 2-terminal measurements while the current is also measured at the same two contacts. In 2-terminal measurements current flow causes an electric potential drop across the two test leads (source and drain) and the contact interface so that the resistance of the contacts is inseparable from the device under test. However, in 4-terminal configuration, one pair of contacts [outer pair, source and drain in Fig. 1(a)] provide the current and other pair of contacts V_1 and V_2 are used to sense the potential drop across the device. In the 4-terminal case there is no current flow through the remote voltage-measuring leads and therefore no electric potential drop across the voltage contacts, thus the effects of contact resistance are eliminated from the measurement. The contact resistance R_c was extracted at V_{ds} = 200 mV from the gate sweep data. In equation (2) $R_{2T} = V_{ds}/I_{2T}$ is the total resistance of the channel including the effect of two metal contacts and $R_{4T} = V_{ds}/I_{4T}$ is the total resistance of the channel when the effect of the two metal contacts are eliminated. Therefore, $R_{2T} - R_{4T}$ provides the contact resistance of the two metal contacts and $(R_{2T} - R_{4T})/2$ yields the contact resistance of each metal contact from the device. Figure 4 (a) demonstrates that the R_c have significant effect on the low gate voltage, where the transistor is in OFF state. The contact resistance without illumination is 450 KΩ at V_{bg} = 10 V, and 100 KΩ at V_{bg} = 50 V. When the channel is illuminated by light, more carriers are generated and conducted through the MoS_2 channel, which reduces the barrier height at the contacts. For 2.27 nW of white light illumination, contact resistance at V_{bg} = 10 V is reduced to 200 KΩ, which is 2.25 times smaller compared to the case without light illumination.

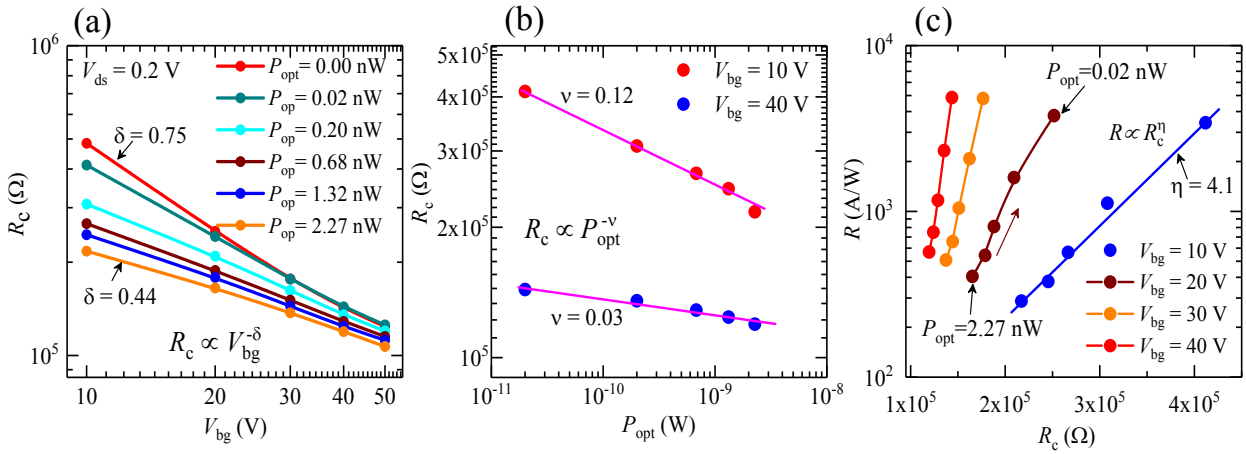

FIG. 4: Display the contact resistance of the device extracted from the measurements of current vs gate voltage and applied optical power. (a) Contact resistance as a function of applied gate voltage at several constant applied optical power. (b) Display the same contact resistance as a function of illuminated optical power at constant gate voltage V_{bg} = 10 V and 40 V. The solid lines in both graphs are the power law fit from where the values of the exponents are extracted. (c) Photoresponsivity, R measured in 4-

terminal method as a function of contact resistance, R_c of the device in logarithmic scale at several constant applied gate voltage.

The contact resistance does not significantly depend upon the light intensity at high gate voltage, since most of the carriers are already populated at the interface with high enough applied gate voltage so that the illumination does not increase the number of carriers in the channel. The R_c value was fitted with a power law of the form $R_c \propto V_{bg}^{-\delta}$. The δ value indicates how the intensity of the illumination affects the contact resistance. The δ value extracted from the power law fitting varies from 0.75 (when no light is shining on the device) to the value 0.44 (when illuminating the device with P_{opt} = 2.27 nW optical signal). We also plotted R_c as a function of the optical power at fixed gate voltages as depicted in Fig. 4 (b). The solid (magenta) lines are fit to the experimental data with the power law $R_c \propto P_{opt}^{-\nu}$. As expected, R_c values are less dependent upon the optical power at high gate voltage (blue dots) or when the transistor is in the ON state compared to the OFF state (red dots). The exponent ν has values of 0.12 at V_{bg} = 10 V and 0.03 at V_{bg} = 40 V. The contact resistance could also be improved using 2D metal contacts such as graphene or similar metallic 2D crystals [52-54]. We also extracted the relationship between photoresponsivity, R and the contact resistance R_c of the device as shown in the Fig. 4 (c). We have the relation of responsivity as a function of P_{opt} know as $R \propto P_{opt}^{-\gamma}$ from device #1 presented in supporting information Fig. S3 (a) and S3 (b) at fixed gate voltage. We also have the similar power law relation of contact resistance, R_c with P_{opt} at a fixed gate voltage $R_c \propto P_{opt}^{-\nu}$. We extracted the relation between R and R_c as $R \propto R_c^{\eta}$, where $\eta = {}^{\gamma}/_{\nu}$ (from the relation $R \propto P_{opt}^{-\gamma}$ and $R_c \propto P_{opt}^{-\nu}$ and also see the Supporting information description of Fig. S7). At V_{bg} = 10 V, we extracted the value of η = 4.1 shown in Fig. 4 (c), which is equal to the value obtained from γ and ν from Fig. S3 (b) and Fig. 4 (b) as $\eta = {}^{\gamma}/_{\nu}$ = 0.53/0.12= 4.4. We also measured the contact resistance as a function of V_{bg} and P_{opt} from the second device #2 [Supporting information Fig. S8 (a)-(c)] and extracted the relationship between photoresponsivity, R and the contact resistance of the device as shown in the supporting Fig. S8 (d). We know $R \propto P_{opt}^{-\gamma}$ from Fig. S7 (c) and S7 (d) at a fixed applied gate voltage. We also have the same power law relation of contact resistance, R_c with P_{opt} at a fixed gate voltage [Fig. S8 (c)]. We extracted the relation between R and R_c as $R \propto R_c^{\eta}$, where $\eta = {}^{\gamma}/_{\nu}$ (See the Supporting information description of Fig. S8). We plotted the R from 4-terminal configuration as a function of R_c in Log-Log scale at several constant V_{bg} for device #2 [Fig. S8 (d)]. Each line shows at constant V_{bg} and increasing function of P_{opt} as shown in the arrow sign in Fig. S8 (d). The data for V_{bg} = 0 was fitted with power law $R \propto R_c^{\eta}$. The exponent extracted from the fitting was η = 5.3, which was close to the value calculated from the exponents γ = 0.71 from 4-terminal measurements [Fig. S7 (c)] and ν = 0.14 [Fig. S8 (c)] as ${}^{\gamma}/_{\nu} = 5.1$.

Although there are several reports that discuss the photoconductivity of MoS_2 and other dichalcogenide compounds using monochromatic light, limited information is available about broadband photodetection to pave the way for a broader range of practical applications. Thus, we extended the present study to explore the optical properties of the MoS_2 photodetector device to the broader spectral range using a customized experimental setup using a Xenon lamp as the light source and a monochromator as a detector as shown in Fig. 5 (a) to study the wavelength dependent photoconductivity. The power delivered to the sample area (channel area) was calculated by measuring the power incident on the device at each and every wavelength that we used for photoconductivity measurements. The photoinduced transfer curves I_{ds} vs V_{bg} are obtained under the illumination of fixed monochromatic lights of spectral range of 400 nm to 900 nm.

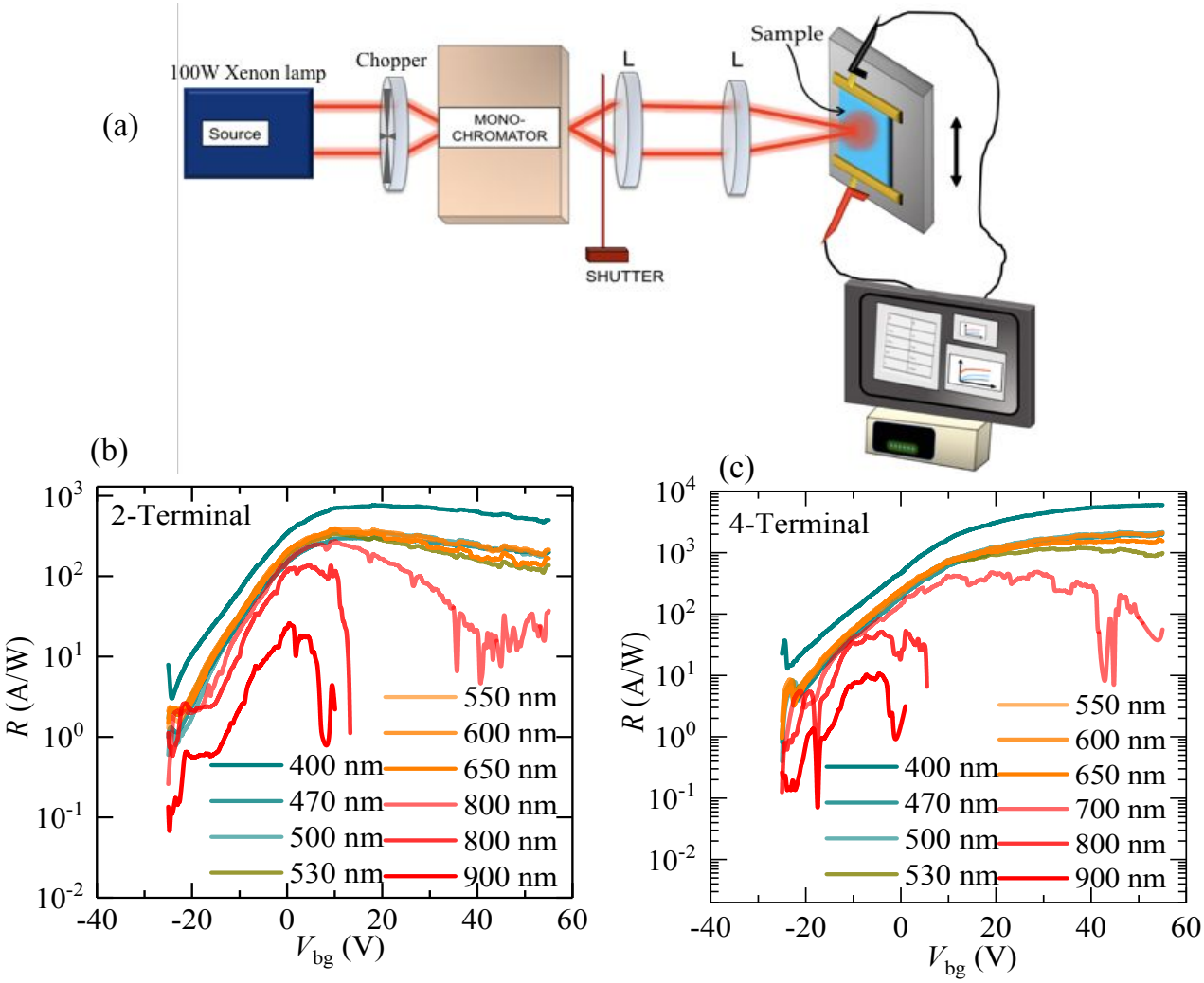

FIG. 5: (a) Schematic of the experimental setup of broadband photoconductivity. (b) and (c) display the responsivities as a function of applied gate voltages at several illuminated wavelengths from 400 nm - 900 nm measured in 2- and 4-terminal configurations respectively. The input optical power on the sample measured from 400 nm to 900 nm wavelengths are 0.16 nW, 0.32 nW, 0.26 nW, 0.23 nW, 0.22 nW, 0.19 nW, 0.16 nW, 0.12 nW, 0.07 nW and 0.2 nW respectively.

The power dependent photocurrent as a function of gate voltage is measured and from there, we extracted the responsivity of the device at several applied gate voltages and plotted it as a function of wavelength. The responsivity as a function of V_{bg} at several constant wavelength measured with 2- and 4-terminal methods are displayed in Fig. 6 (a) and (b) respectively. Similar to the responsivity under white light in Fig. 3 (c), the 2-terminal responsivity increases as a function of V_{bg} and peaks between 0 V and 10 V. The maximum R value measured at 400 nm wavelength between V_{bg} = 0-10 V then decreased slowly with increasing wavelength into the IR wavelength range, which is similar to the reported results by Lee et al. [30]. The highest 2-terminal responsivity observed in our multi-layered MoS_2 devices is ~ 800 A/W at a wavelength of 400 nm. The responsivity decreases with increasing wavelength as shown in Fig. 5 (b). The gate voltage dependent responsivity measured in 4-terminal configuration is depicted in Fig. 5 (c). As mentioned previously, measurements performed in 4-terminal configurations show much higher responsivities (by an order of magnitude) compared to the responsivity extracted from the 2-terminal measurements. The responsivity increases continuously as a function of increasing gate voltage and reaches 6×10^3 A/W at V_{bg} = 55 V. The photodetector shows higher R in the ON state of the transistor compared to the OFF state which is in agreement with the results reported by Lee and coworkers [30].

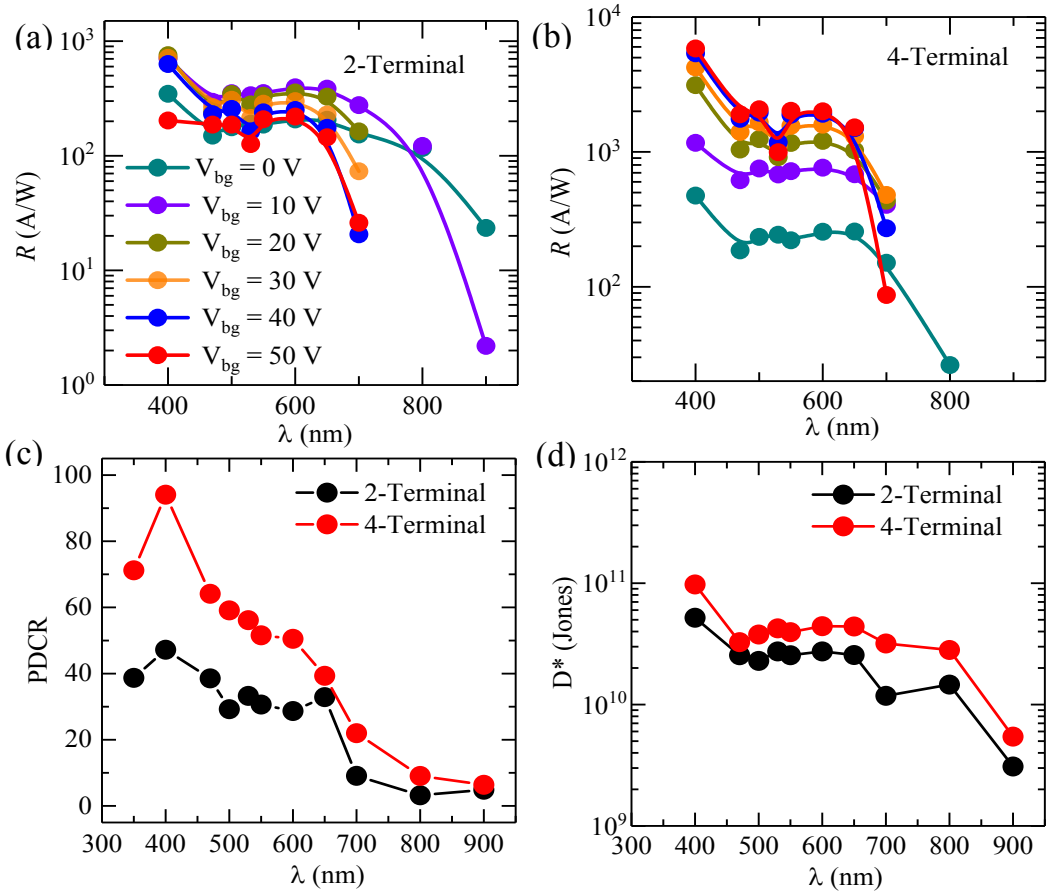

FIG. 6: (a) and (b) display the photoresponsivity as a function of incident wavelength measured in 2- and 4-terminal configurations respectively at several applied gate voltages. (c) Display the PDCR

values extracted from (a) and (b) for both 2- and 4-terminal measurements. (d) Display the detectivity of the photodetector device as a function of wavelength.

In the near infrared region, few-layered MoS_2 has very low absorption due to the nature of its indirect band-gap and band-edge. Due to the weak absorption, it is difficult to measure the response from the sample. The missing data are due to the uncertainty of measuring the photocurrent above a certain gate voltage at wavelengths λ = 800 and 900 nm due to the weak absorption of the material [27,29].

To understand the wavelength dependency of the data, we plotted the responsivity as a function of wavelength from the maximum value or peak position (V_{bg} = 0 to 50 V range) of R vs V_{bg} graph in Fig. 5 (b) & (c) and depicted in Fig. 6 (a) and (b). The highest 2-terminal responsivity (R_{2T}) of our few-layered MoS_2 photodetector measured at 400 nm is 800 A/W and shows a dip at 500 nm. Then R_{2T} shows a broad peak like feature around 600 nm before dropping in value as it approaches the infrared region at 900 nm [shown in Fig. 6 (a)], where it still shows high values of R (20 A/W) and gate voltage dependency. All the gate voltage dependent responsivity data shows a similar trend of wavelength dependence while also matching the absorption spectrum of the crystalline MoS_2 materials [55-57]. The broad peak like feature in R from 600 nm to 700 nm at low energy is due to the A and B excitonic transitions between the maximum of the valence band and the minimum of the conduction band at the K-point of the Brillouin zone for MoS_2 nanosheets [9]. The responsivity extracted from the 4-terminal measurements is shown in Fig. 6 (b) as a function of wavelength at several constant back gate voltages. The highest responsivity measured is ~ 6000 A/W under 400 nm illumination compared to its 2-terminal value, which is an order of magnitude smaller. The overall response of the responsivity and its wavelength dependence is similar to the 2-terminal measurements. These results show the impact of contact resistance on the transport properties of the device, particularly in few atomic layers of TMDs. The responsivity near infrared is still high ~ 100-500 A/W. The responsivity slowly decreased above V_{bg} = 10 V for the entire spectral range when measured using the 2-terminal method [Fig. 6 (a)]. On the other hand, the responsivity increased monotonically until V_{bg} = 40 V, and saturated at V_{bg} = 50 V when measured in 4-terminal configuration [Fig. 6 (b)]. Due to the weak absorption for few-layered MoS_2 in the near-IR region as discussed before, it was difficult to extract the photocurrent precisely for λ >700 nm. The responsivity showed a sharp decrease above 650 nm due to the low absorption of the indirect band gap of MoS_2 in the near-IR region. This suggests the few layered MoS_2 can be used in broadband photodetection applications where the metal contacts to 2D materials are less affected by the contact resistance, which increases the charge collection efficiency at the metal-semiconductor interface resulting in better performance. The use of graphene for source and drain contacts reported by Lee and coworkers show good efficiency of current injection due to the minimization of the contact resistance [58]. Similarly, Kim and coworkers used graphene as the contact electrode to enhance the collection of charge in vertical MoS_2/WSe_2 p-n junction solar cell [52]. The external quantum

efficiency (EQE) is another figure-of-merit, which is defined as the ratio of number of electron-hole pairs created to the number of incident photons. High EQE values would indicate suitability for light-to-current conversion applications. The maximum EQE values extracted from the device range from 10^5 to 10^6 % (Supporting information Fig. S4).

In addition to Responsivity and EQE, another figure-of-merit used to quantify photodetector performance is the photocurrent-to-dark current ratio (PDCR). PDCR is a measure of the photodetector sensitivity with respect to the dark current (also called leakage current). We extracted the PDCR values for both 2- and 4-terminal measurements [shown in Fig. 6 (c)] using the relation below for the entire wavelength range included in our study,

$$PDCR = \frac{I_{ph} - I_{dark}}{I_{dark}} \qquad (3)$$

The highest PDCR value obtained from our device is 90 and 50 for 4- and 2-terminal methods respectively at 400 nm and it decreases to 5 at IR, λ= 900 nm. These values are much higher than those obtained using the traditional photodetectors currently in use such as AlN, GaN, SiC, Ga_2O_3 etc [59-62]. Tsai and coworker reported a PDCR value of 3000 at room temperature for few layered MoS_2 but at high applied V_{ds} = 5 V. We further evaluated the specific detectivity, which is another important parameter to determine the capability of a phototransistor to respond to a weak light signal, which is also shown in Fig. 6 (d). If the dark current is considered to be the single major contributor to the noise current, then the detectivity can be calculated using the following formula

$$D^* = R \times \sqrt{\frac{A}{2qI_{dark}}} \qquad (4)$$

where R is the photoresponsivity, A and q are the channel area of the detector and electron charge (q=1.6×10 ^{19} C) respectively. The detectivity of the device measured in 4-terminal is slightly higher than that measured using the 2-terminal method. The highest detectivity measured at λ = 400 nm is 10^{11} Jones and decreases slowly to the value of 5×10^9 Jones at λ = 900 nm. Our few-layered MoS_2 photodetector's detectivity at visible range is slightly higher than the reported value for a 60 nm thick MoS_2 phototransistor reported by Choi et al. and two orders of magnitude higher in the IR region [28]. These discrepancies could be attributed to contributions from contact resistance, applied bias voltage etc. Similar to the responsivity, the PDCR and detectivity values measured in the near-infrared region showed a sharp decrease due to the weak absorption of the few-layered MoS_2 crystals. The PDCR values extracted from 4-terminal measurements were much higher than the 2-terminal values in the visible region and became closer when the device operated in the near-IR region.

IV. CONCLUSION

We explored the broadband photodetection on few-layered MoS_2 phototransistor encapsulated with Cytop fabricated on a p-doped Si/SiO_2 substrate. The photoconductivities are measured using the conventional 2-terminal as well as 4-terminal methods to observe the intrinsic phototransport properties. We compared the results obtained from white light and monochromatic light illumination ranges from λ = 400 nm - 900 nm. The devices exhibit high responsivity in white light as well as under monochromatic light illumination. An order of magnitude increase in the responsivity was observed when we measured in 4-terminal method due to the elimination of contact resistance between the semiconductor MoS_2 and metal contacts. We extracted the contact resistance, which clearly indicates the dependencies of photoresponsivity on few-layered MoS_2. The responsivity as a function of contact resistance clearly indicates the intrinsic photoconductivity affected by metal contacts. We also observed high photoresponsivity and EQE as a function of applied gate voltage. We observed *R* values as high as 6×10^3 A/W at λ = 400 nm which decreases to 20 A/W in the IR region at λ = 900 nm. The observed EQE value is as high as 2×10^6 % measured in a 4-terminal configuration, which is an order of magnitude higher than the 2-terminal measurements. This suggests that our measurement in 4-terminal method provides the value of the intrinsic photoconductivity, which was extracted by eliminating the contact resistance. Further we also presented in detail the PDCR and detectivity of the device as a function of wavelength from 400 nm to 900 nm, showing that, the few-layered MoS_2 could be a suitable candidate for broadband photodetection when appropriate contacts are used by reducing the contact resistance of the device which enhances the responsivity and providing the intrinsic physical properties of the material. The broadband photosensitivity can be further enhanced using plasmonic nanoparticles and/or heterostructure devices using different types of 2D materials with varying bandgaps.

IV. METHOD

Fabrication, Electrical and Optical Measurements: Few layered MoS_2 flakes were exfoliated using blue Nito tape (product #SPV 224 PR-M) and then transferred on to a clean SiO_2 substrate with 285 nm thick oxide layer. Metal contacts were fabricated using Laser writer (Model # LW405) and Cr/Au (5nm/ 80nm) were deposited using Lesker e-beam evaporator at 10^{-8} torr vacuum pressure. The devices were encapsulated with ~20 nm thick Cytop layer (amorphous fluoropolymer). Keithley instruments 2612B and 2635 source meters were used to perform electrical measurements. A white light source using Motic MLC-150 C halogen fiber optic illuminator was used for white light measurements and a Xenon lamp coupled with a monochromator was used for broadband photoconductivity measurements from λ= 400 nm to 900 nm. The 2-terminal method was performed using two contacts, source (S) and drain (D) contacts shown in Fig. 1(a), where both current and voltage drop were measured at the same contacts. On the other hand, in 4-terminal measurements while current measured at S and D contacts,

voltage was sense through two separate terminals V_1 and V_2. Thus the 4-terminal measurements eliminates the effect of contact resistance associated with the 2-terminal method. The same V_{ds} applied to the source to drive the accumulated charge carriers as applied in 2-terminal method but it senses the voltage drop using V_1 and V_2 terminals.

Raman Measurements: The Raman measurements of several MoS_2 crystals with different thickness were performed using a Renisha inVia Raman setup at room temperature and in ambient condition.

Author Contributions

NRP conceived the project. NRP, VMN and DK synthesize the material. NRP, SAM, BT, DR (Raghavan) and AVS did the Raman measurement of exfoliated flakes. NRP, RB, MW, DR (Rosenmann), RD and AVS fabricated the transistor devices. NRP, PD, JN, MW, SAM, QD and PCR performed the electrical and optical transport measurement. NRP, PD, JN, GG and AK analyzed the data. NRP wrote the manuscript with the input of all co-authors.

Conflicts of interest

The authors declare no competing financial interests.

Acknowledgments

This work was performed, in part, at the Center for Nanoscale Materials, a U.S. Department of Energy Office of Science User Facility, and supported by the U.S. Department of Energy, Office of Science, under Contract No. DE-AC02-06CH11357. N. R. P. acknowledged NSF-PREM through NSF-DMR-1826886, HBCU-UP Excellence in research NSF-DMR-1900692. A portion of this work was performed at the National High Magnetic Field Laboratory, which is supported by National Science Foundation Cooperative Agreement No. DMR-1644779 and the State of Florida.

Electronic Supplementary Information: The supplementary materials include the Raman measurements in Fig. S1, photocurrent comparison between 2-terminal and 4-terminal measurements in Fig. S2, comparison of photoconductivity parameter of several reported results on MoS_2 presented in Table -1, responsivity as a function of optical power in Fig. S3 and EQE results from device #1 in Fig. S4. A detail study of electrical properties, photocurrents, photoresponsivity and contact resistance, responsivity as a function of contact resistance from a second device #2 are also presented in the Figs. S5-S8.

References:

1. J. Kallhammer, *Nat. Photon.* 2006, **5**, 12-13.
2. F. C. Lussani, R. F. d. C. Vescovi, T. D. d. Souza, C. A. Leite, and C. Giles, *Rev. Sci. Instrum.* 2015, **86**, 063705 (1-8).
3. R. A. Bartels, A. Paul, H. Green, H. C. Kapteyn, M. M. Murnane, S. Backus, I. P. Christov, Y. Liu, D. Attwood, and C. Jacobsen, *Science* 2002, **297**, 376-378.
4. B. J. Zeskind, C. D. Jordan, W. Timp, L. Trapani, G. Waller, V. Horodincu, D. J. Ehrlich, and P. Matsudaira, *Nat. Methods*. 2007, **4**, 567-569.
5. X. Qian, X.-H. Peng, D. O. Ansari, Q. Yin-Goen, G. Z. Chen, D. M. Shin, L. Yang, A. N. Young, M. D. Wang, and S. Nie, *Nat. Biotechnol.* 2008, **26**, 83-90.
6. V. Formisano, S. Atreya, T. Encrenaz, N. Ignatiev, and M. Giuranna, *Science* 2004, **306**, 1758-1761.
7. B. Fowler, C. Liu, S. Mims, J. Balicki, W. Li, H. Do, J. Appelbaum, and P. Vu, *Sensors, Cameras, and Systems for Industrial/Scientific Applications XI (International Society for Optics and Photonics)* 2010, **7536**, 753607 (1-12).
8. T. Chu, H. Ilatikhameneh, G. Klimeck, R. Rahman, and Z. Chen, *Nano lett.* 2015, **15**, 8000-8007.
9. K. F. Mak, C. Lee, J. Hone, J. Shan, and T. F. Heinz, *Phys. Rev. Lett.* 2010, **105**, 136805 (1-4).
10. S. B. Desai, G. Seol, J. S. Kang, H. Fang, C. Battaglia, R. Kapadia, J. W. Ager, J. Guo, and A. Javey, *Nano Lett.* 2014, **14**, 4592-4597.
11. L. Britnell, R. Ribeiro, A. Eckmann, R. Jalil, B. Belle, A. Mishchenko, Y.-J. Kim, R. Gorbachev, T. Georgiou, S. Morozov, A. N. Grigorenko1, A. K. Geim, C. Casiraghi, A. H. Castro Neto, and K. S. Novoselov, *Science* 2013, **340**, 1311-1314.
12. U. Wurstbauer, B. Miller, E. Parzinger, and A. W. Holleitner, *J. Phys. D Appl. Phys.* 2017, **50**, 173001(1-19).
13. B. Chakraborty, J. Gu, Z. Sun, M. Khatoniar, R. Bushati, A. L. Boehmke, R. Koots, and V. M. Menon, *Nano lett.* 2018, **18**, 6455-6460.
14. Z. Yin, H. Li, H. Li, L. Jiang, Y. Shi, Y. Sun, G. Lu, Q. Zhang, X. Chen, and H. Zhang, *ACS nano* 2012, **6**, 74-80.
15. O. Lopez-Sanchez, D. Lembke, M. Kayci, A. Radenovic, and A. Kis, *Nat. Nanotechnol.* 2013, **8**, 497- 501.
16. N. Perea-Lopez, Z. Lin, N. R. Pradhan, A. Iniguez-Rabago, A. L. Elias, A. McCreary, J. Lou, P. M. Ajayan, H. Terrones, L. Balicas, and M. Terrones, *2D Mater.* 2014, **1**, 011004 (1-11).

17. N. R. Pradhan, C. Garcia, J. Holleman, D. Rhodes, C. Parker, S. Talapatra, M. Terrones, L. Balicas, and S. A. McGill, *2D Mater.* 2016, **3**, 041004 (1-11).
18. N. R. Pradhan, J. Ludwig, Z. Lu, D. Rhodes, M. M. Bishop, K. Thirunavukkuarasu, S. A. McGill, D. Smirnov, and L. Balicas, *ACS Appl. Mater. Interfaces* 2015, **7**, 12080-12088.
19. C. Garcia, N. R. Pradhan, D. Rhodes, L. Balicas, and S. McGill, *J. Appl. Phys.* 2018, **124**, 204306 (1-6).
20. R. Walker, T. Shi, E. Silva, I. Jovanovic, and J. Robinson, *Phys. Status Solidi A* 2016, **213**, 3065- 3077.
21. S. Ghosh, M. Wasala, N. R. Pradhan, D. Rhodes, P. D. Patil, M. Fralaide, Y. Xin, S. A. McGill, L. Balicas, and S. Talapatra, *Nanotechnology* 2018, **29**, 484002 (1-16).
22. M. Rivera, R. Velazquez, A. Aldalbahi, A. F. Zhou, and P. Feng, *Sci. Rep.* 2017, **7**, 42973 (1-10).
23. S.-H. Jo, H. W. Lee, J. Shim, K. Heo, M. Kim, Y. J. Song, and J.-H. Park, *Adv. Sci.* 2018, **5**, 1700423 (1-9).
24. E. Zhang, Y. Jin, X. Yuan, W. Wang, C. Zhang, L. Tang, S. Liu, P. Zhou, W. Hu, and F. Xiu, *Adv. Funct. Mater.* 2015, **25**, 4076- 4082.
25. E. Liu, M. Long, J. Zeng, W. Luo, Y. Wang, Y. Pan, W. Zhou, B. Wang, W. Hu, Z. Ni, Y. You, X. Zhang, S. Qin, Y. Shi , K. Watanabe, T. Taniguchi, H. Yuan, H. Y. Hwang , Y. Cui , F. Miao, and D. Xing, *Adv. Funct. Mater.* 2016, **26**, 1938-1944.
26. R. M. Tanthirige, C. Garcia, S. Ghosh, F. J. II, J. Nash, D. Rosenmann, R. Divan, L. Stan, A. V. Sumant, S. A. McGill, P. C. Ray, and N. R. Pradhan, *Semiconductor Science and Information Devices* 2020, **1**, 19-28.
27. W. Choi, M. Y. Cho, A. Konar, J. H. Lee, G.-B. Cha, S. C. Hong, S. Kim, J. Kim, D. Jena, J. Joo, and S. Kim, *Adv. Mater.* 2012, **24**, 5902.
28. W. Choi, M. Y. Cho, A. Konar, J. H. Lee, G.-B. Cha, S. C. Hong, S. Kim, J. Kim, D. Jena, J. Joo, and S. Kim, *Adv. Mater.* 2012, **24**, 5832- 5836.
29. D.-S. Tsai, K.-K. Liu, D.-H. Lien, M.-L. Tsai, C.-F. Kang, C.-A. Lin, L.-J. Li, and J.-H. He, *Acs Nano* 2013, **7**, 3905- 3911.
30. Y. T. Lee, J.-H. Kang, K. Kwak, J. Ahn, H. T. Choi, B.-K. Ju, S. H. Shokouh, S. Im, M.-C. Park, and D. K. Hwang, *ACS Photonics* 2018, **5**, 4745- 4750.
31. X. Zhang, F. Lou, C. Li, X. Zhang, N. Jia, T. Yu, J. He, B. Zhang, H. Xia, S. Wang, and X. Tao, *CrystEngComm* 2015, **17**, 4026- 4032.
32. A. Yoon and Z. Lee, *Appl. Microsc.* 2017, **47**, 19-28.
33. N. R. Pradhan, D. Rhodes, Y. Xin, S. Memaran, L. Bhaskaran, M. Siddiq, S. Hill, P. M. Ajayan, and L. Balicas, *Acs Nano* **8**, 7923- 7929.

34. N. R. Pradhan, A. McCreary, D. Rhodes, Z. Lu, S. Feng, E. Manousakis, D. Smirnov, R. Namburu, M. Dubey, A. R. Hight Walker, H. Terrones, M. Terrones, V. Dobrosavljevic, and L. Balicas, *Nano lett.* 2015, **15**, 8377-8384.
35. N. Pradhan, D. Rhodes, S. Memaran, J. Poumirol, D. Smirnov, S. Talapatra, S. Feng, N. Perea-Lopez, A. Elias, M. Terrones, P. M. Ajayan, and L. Balicas, *Sci. Rep.* 2015, **5**, 8979 (1-8).
36. N. R. Pradhan, C. Garcia, M. C. Lucking, S. Pakhira, J. Martinez, D. Rosenmann, R. Divan, A. V. Sumant, H. Terrones, J. L. Mendoza-Cortes, S. A. McGill, N. D. Zhigadlo, and L. Balicas, *Nanoscale* 2019, **11**, 18449-18463.
37. Q. Wang, Y. Shao, P. Gong, and X. Shi, *J. Mater. Chem. C* 2020, **8**, 3113-3119.
38. S. Choi, Z. Shaolin, and W. Yang, *J. Korean Phys. Soc.* 2014, **64**, 1550- 1555.
39. M. Farmanbar and G. Brocks, *Phys. Rev. B*, 2016, **93**, 085304 (1-12).
40. J. Kang, W. Liu, D. Sarkar, D. Jena, and K. Banerjee, *Phys. Rev. X*, 2014, **4**, 031005 (1-14).
41. N. Pradhan, D. Rhodes, Q. Zhang, S. Talapatra, M. Terrones, P. Ajayan, and L. Balicas, *Appl. Phys. Lett.* 2013, **102**, 123105 (1-4).
42. B. Radisavljevic, A. Radenovic, J. Brivio, V. Giacometti, and A. Kis, *Nat. Nanotechnol.* 2011, **6**, 147-150.
43. H. Wang, L. Yu, Y.-H. Lee, Y. Shi, A. Hsu, M. L. Chin, L.-J. Li, M. Dubey, J. Kong, and T. Palacios, *Nano lett.* 2012, **12**, 4674-4680.
44. S. Das, H.-Y. Chen, A. V. Penumatcha, and J. Appenzeller, *Nano lett.* 2013, **13**, 100-105.
45. S. H. Song, M.-K. Joo, M. Neumann, H. Kim, and Y. H. Lee, *Nat. Nanotechnol.* 2017, **8**, 1-6.
46. J. Hong, Z. Hu, M. Probert, K. Li, D. Lv, X. Yang, L. Gu, N. Mao, Q. Feng, L. Xie, J. Zhang, D. Wu, Z. Zhang, C. Jin, W. Ji, X. Zhang, J. Yuan, and Z. Zhang, *Nat. Commun* 2015, **6**, 1-8.
47. R. Yang, Z. Wang, and P. X.-L. Feng, *Nanoscale* 2014, **6**, 12383-12390.
48. M.-Y. Ryu, H.-K. Jang, K. J. Lee, M. Piao, S.-P. Ko, M. Shin, J. Huh, and G.-T. Kim, *Phys. Chem. Chem. Phys.* 2017, **19**, 13133-13139.
49. S. Kim, A. Konar, W.-S. Hwang, J. H. Lee, J. Lee, J. Yang, C. Jung, H. Kim, J.-B. Yoo, J.-Y. Choi, Y. W. Jin, S.Y. Lee, D. Jena, W. Choi, and K. Kim, *Nat. Commun* 2012, **3**, 1-7.
50. R. K. Ulaganathan, Y.-Y. Lu, C.-J. Kuo, S. R. Tamalampudi, R. Sankar, K. M. Boopathi, A. Anand, K. Yadav, R. J. Mathew, C.-R. Liu, F. C. Choue, and Y.-T. Chen, *Nanoscale* 2016, **8**, 2284-2292.
51. S. Rashkeev, D. Fleetwood, R. Schrimpf, and S. Pantelides, *Phys. Rev. Lett.* 2001, **87**, 165506 (1-4).
52. C.-H. Lee, G.-H. Lee, A. M. v. d. Zande, W. Chen, Y. Li, M. Han, X. Cui, G. Arefe, C. Nuckolls, T. F. Heinz, J. Guo, J. Hone, and P. Kim, *Nat. Nanotechnol.* 2014, **9**, 676- 681.
53. S. Andleeb, J. Eom, N. R. Naz, and A. K. Singh, *J. Mater. Chem.C* 2017, **5**, 8308-8314.

54. Y. Liu, H. Wu, H.-C. Cheng, S. Yang, E. Zhu, Q. He, M. Ding, D. Li, J. Guo, N. O. Weiss, Y. Huang, and X. Duan, *Nano lett.* 2015, **15**, 3030-3034.
55. V. Forsberg, R. Zhang, J. Backstrom, C. Dahlstrom, B. Andres, M. Norgren, M. Andersson, M. Hummelgard, and H. Olin, *PloS One* 2016, **11**, 1-12.
56. S. Mukherjee, R. Maiti, A. Midya, S. Das, and S. K. Ray, *Acs Photonics* 2015, **2**, 760-768.
57. L. Li, J. Chen, K. Wu, C. Cao, S. Shi, and J. Cui, *Nanomaterials* 2019, **9**, 1366 (1-11).
58. Y. T. Lee, K. Choi, H. S. Lee, S.-W. Min, P. J. Jeon, D. K. Hwang, H. J. Choi, and S. Im, *Small* 2014, **10**, 2356-236.
59. H. So and D. G. Senesky, *Appl. Surf. Sci.* 2016, **387**, 280-284.
60. D.-S. Tsai, W.-C. Lien, D.-H. Lien, K.-M. Chen, M.-L. Tsai, D. G. Senesky, Y.-C. Yu, A. P. Pisano, and J.-H. He, *Sci. Rep.* 2013, **3**, 2628 (1-5).
61. W.-C. Lien, D.-S. Tsai, S.-H. Chiu, D. G. Senesky, R. Maboudian, A. P. Pisano, and J.-H. He, *IEEE Electron Device Lett.* 2011, **32**, 1564-1566.
62. T.-C. Wei, D.-S. Tsai, P. Ravadgar, J.-J. Ke, M.-L. Tsai, D.-H. Lien, C.-Y. Huang, R.-H. Horng, and J.-H. He, *IEEE J. Sel. Top. Quantum Electron.* 2014, **20**, 3802006.